

Morphological analysis of organo-montmorillonites via MD simulations

Deniz Karataş^{1,4}, Adem Tekin², Muhammed F. Can^{3,4}, Zhenghe Xu⁴, Mehmet S. Çelik¹

¹ Istanbul Technical University, Mineral Processing Engineering Department, 34469, Maslak, Istanbul, Turkey

² Informatics Institute, Istanbul Technical University, 34469 Maslak, Istanbul, Turkey

³ Afyonkocatepe University, Engineering Faculty, Mining Engineering Dept., 03200, Afyonkarahisar, Turkey

⁴ Department of Chemical and Materials Engineering University of Alberta, Edmonton, Alberta, Canada, T6G 2G6

Corresponding author: karatasde@itu.edu.tr (Deniz Karataş)

Abstract: Adsorption on clay surfaces has been studied intensively in recent years. The most curious subject of these studies, which are generally experimental, is how the surfactants are adsorbed at the atomic level to the surface. In this study, the adsorption of quaternary amine salt (tetradecyl dimethyl ethyl benzyl ammonium chloride-TDEBAC) to sodium montmorillonite (Na-MMT) with various cation exchange capacities (CEC) was investigated by using Molecular Dynamics (MD) simulation. In the simulations, as in the experimental studies, it was revealed that the surfactants were both adsorbed on to basal surfaces and settled between the layers. From the morphological analysis obtained from MD simulations, it was calculated that the inter-molecular interaction between the layers was higher than on the basal surface. For example, for the model with 118 CEC motif, the binding energy of all three surfactants in the models with the hydrophilic heads facing the same direction was calculated as -678.18 kcal/mol at the basal surface, while this value was found to be -688.90 kcal/mol in the interlayer. The more striking result is that in the simulations made by turning the head of the middle one of the three surfactants towards the tails of the right and left ones, only -34.86 kcal/mol binding energy was calculated on the basal surface, while this value was -525.63 kcal/mol in the interlayer. As compared middle reversed surfactant models with the same direction ones, despite increased CEC the intermolecular interaction decreased for the basal surface, but the interaction increased between the layers.

Keywords: organo-montmorillonite, tetradecyl dimethyl ethyl benzyl ammonium chloride, molecular dynamics simulation, cation exchange capacity, binding energy

1. Introduction

Clay minerals are used in various industrial applications due to their low cost, high cation exchange capacity, high surface area, adsorption properties, and naturally hydrophilic surfaces (Breen et al., 1997). Montmorillonite (MMT) is a hydro-silicate clay mineral with layered structure consisting of silica tetrahedron (SiO₄) and alumina octahedron (AlO₆) sheets within the general chemical formula of (Na,Ca)_{0,3}(Al,Mg)₂Si₄O₁₀(OH)₂•n(H₂O) (Viani et al., 2002). MMT is 2:1 phyllosilicate clay presenting permanent layer charge due to the faulted edges and isomorphous substitutions. The isomorphous substitution in the tetrahedral sheet between silicon (Si⁺⁴) and aluminum (Al⁺³), and magnesium (Mg⁺²) substitution for aluminum (Al⁺³) in the octahedral sheet impart cation exchange capacity (CEC) (He et al., 2010). After substitution, the excess of negative charge in MMT is neutralized by some cations like sodium (Na⁺) and calcium (Ca⁺²) through electrostatic interactions. Experimental investigations generally indicate that MMT has CEC value of 80-150 meq/100 g. Hang and Brindley (Hang and Brindley, 1970) stated that using the methylene blue (MB) method, Na- MMT of Wyoming region yielded a CEC value of 126 ± 2 meq/100 g.

Montmorillonite or with its commercial name bentonite is generally not directly used in industrial applications. In addition to its diverse applications, it is also used as organically modified clay

(organoclay) in nanocomposite production. Organoclay is obtained by some surface-active agents especially quaternary amine salts to make surface hydrophobic (water repelling) and to increase the basal space (interlayer) of MMT type clays. On the other hand, MMT with a high CEC capacity can adsorb more surfactant due to its high surface area. Accordingly, in recent years its industrial use has increased particularly in the preparation of polymer nanocomposite to reduce the surface energy of clay. For example, addition of organoclays into polymeric matrices improved mechanical, physical (thermal and barrier) and chemical properties of the matrices and reduced cost in some cases (de Paiva et al., 2008; Markarian, 2005). Most popular application areas of organoclays are removal of pollutants from water and soil (Theng et al., 2008), adsorbents, rheological control agents, paints, grease, cosmetics, personal care products, and oil well drilling fluids (Maes et al., 1979). These products generally are prepared by cation exchange reactions in aqueous solution. On the other hand, solid state reactions are prepared with organoclays in the absence of any kind of liquid (Merinska et al., 2002; Yoshimoto et al., 2005). Organo-montmorillonite which exhibits more swelled and intercalated structure is characterized by CEC, XRD, FT-IR, TGA (Thermo Gravimetric Analysis) and swelling index in organic solvents. Most of the above instrumental characterization methods such as XRD, FT-IR, and CEC can be also modeled and simulated by theoretical studies. Molecular Dynamics (MD) is one of the computational simulations to better understand inter/intra molecular interactions at atomistic level. It is a tool that enables the interpretation of experimental studies (Zhao and Burns, 2012) and consists of quantitative information and thermodynamic properties of simulated systems (Liu et al., 2009). For instance, Tanaka and Goettler (Tanaka and Goettler, 2002) calculated the binding energy of 6,6 nylon for one montmorillonite layer and concluded that the binding energies of the composite decreased as the volume of the adsorbed surfactant increased. Another similar study (Fermeglia et al., 2003) on nylon 6 and montmorillonite platelet in the presence of quaternary ammonium salt showed that the head groups of amine are distributed within two layers, whereas the distributions of methyl and methylene are strongly dependent on the chain length and clay layer charge. Further, simulation of quaternary ammonium salts against increasing surfactant chain length increased MMT surface charge and basal spacing as well (Zeng et al., 2003). Although all of these molecular dynamics simulation studies have explained the mechanism of adsorption and structural behavior of MMT layer, solvation effect on intercalation and swelling behavior of clay were not mentioned due to the absence of water molecules in the medium. Simulations were basically run as a solid-state modification of MMT. Since many technological applications require aqueous phase, determination of the role of water during organoclay production must be understood at the atomistic level.

The main objective of this study is therefore to understand importance and effect of explicit water molecules on adsorption of quaternary amines onto MMT. Toward this aim, a sodium montmorillonite supercell with different CEC values using a quaternary ammonium surfactant (tetradecyl dimethyl ethyl benzyl ammonium chloride-TDEBAC) was built and simulated by molecular dynamics (MD) simulations. We selected TDEBAC to explain hydrophobic interactions due to its chain and polar head group effect on intercalation of Na-MMT. For this purpose, some structural, dynamical, and statistical analysis such as basal spacing, radial distribution function (RDF), mean square displacement (MSD) and intermolecular interactions were investigated. Unlike previous studies, FT-IR, structural behavior of sodium and chloride ions, hydration and free binding energies and effect of the head group of surfactants (including a benzene ring and ethyl group $-\text{CH}_2\text{CH}_3-$) on adsorption mechanism were investigated in the presence of water.

2. Computational methods

2.1. Model construction

In this study, molecular dynamic simulation of intercalation and swelling behavior of Na-MMT in the presence of quaternary ammonium surfactant and water was investigated using Materials Studio package (v 4.2 Accelrys, San Diego, CA, USA, 2007). For this purpose, 2 layers (4x4x2 unit cell) of Na-MMT were built as a supercell within $20 \times 36 \times 200 \text{ \AA}^3$ dimension. Four models were basically generated to understand the mechanism of adsorption and intercalation of Na-MMT. One includes no substitution, and the remaining models were built by means of unit cell formula (Fermeglia et al., 2003) given below in conjunction with different CEC ratios.



Here, M represents sodium (Na) and x denotes the layer charge. As ' x ' equals to 0.625, 0.875 and 1.125, the molecular weight of the models came out to be 733.32, 738.40 and 743.48 g/mol, respectively. Accordingly, CEC was approximately calculated as 85, 118 and 151 meq/100g; this means that a total of 10, 14 and 18 substitutions for one layer of Na-MMT were calculated in place of Mg^{2+} for Al^{3+} in the octahedral sheet (Heinz and Suter, 2004) and in place of Al^{3+} for Si^{4+} in the tetrahedral (Zeng et al., 2003) sheet. The ratio of substitutions was selected as 40/60 for tetrahedral/octahedral to explain isomorphous substitution behavior on basal spacing. All entire substitutions were made for negatively charged surfaces. Na^+ cations were added to the models both in the interlayer and basal surface of Na-MMT to neutralize the total charge. As illustrated in Fig. 1, the total surface charges were calculated as -0.2, 0.0, -0.3 and 0.0 electron (e) for no substitution, 85, 118 and 151 meq/100g models, respectively. Thus, the final chemical composition of models are $(Na_{0.625})Si_8[(Al_{3.375})(Mg_{0.625})O_{20}(OH)_{4.n}(H_2O)_n]$, $(Na_{0.875})Si_8[(Al_{3.125})(Mg_{0.875})O_{20}(OH)_{4.n}(H_2O)_n]$, and $(Na_{1.125})Si_8[(Al_{2.875})(Mg_{1.125})O_{20}(OH)_{4.n}(H_2O)_n]$.

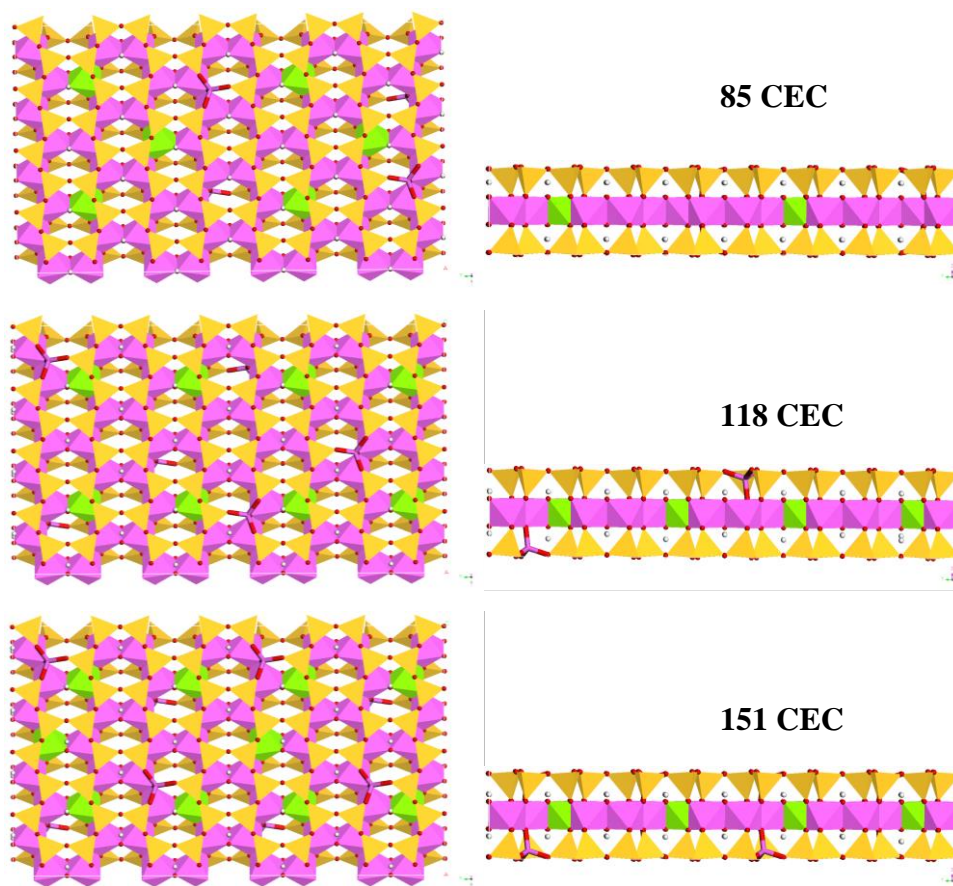


Fig. 1. Top (left) and side (right) views of the Na-MMT supercell displayed as polyhedron style within different CEC ratios. Colors representing red (oxygen); white (hydrogen); yellow (silicon); green (magnesium); and pink (aluminum), (8, 10 Mg substituted for Al in the 118, 151 CEC configuration, respectively, seen in the left side caption)

The number of surfactant molecules packing into Na-MMT was then computed. Since the basal surface area of montmorillonite layer is $20.72 \times 35.92 \text{ \AA}^2$ and the dimensions of each surfactant are $4.33 \times 27.61 \text{ \AA}^2$, the maximum packing area of one TDEBAC is approximately 49 \AA^2 ; this indicates that three TDEBAC molecules horizontally cover the full surface of substrate and three of them can jointly penetrate at the same time into the aqueous medium. Theoretically, two configurations of surfactant were thought to get incorporated into the basal surface and interlayer cavity of MMT. The first configuration is that all the three head groups of surfactants are in the same direction and the second one is that the middle surfactant is oppositely directed. Thereby not only surfactant adsorption on montmorillonite surfaces but also chain-chain hydrophobic interactions (Ersoy and Celik, 2003) can be

verified by simulation. Ten water molecules were taken for each unit cell as mentioned in the empirical formula (Viani et al., 2002) to better understand and clarify the adsorption mechanism of quaternary ammonium surfactant on montmorillonite in aqueous medium. Also, for basal surface, 1300 water molecules were constructed by Amorphous Cell module. Two cases were considered: One is to take identical XY dimensions of the cell parameters, and the other is to assume twice of the length of surfactants (27.61 Å). Z dimension was set to 200 Å to neglect H-bond interaction between the upper water layer and MMT back-sheet surface oxygen. In summary, 4 configurations (shown in Fig. 2) for each 4 different CEC clay structures including 1460 water molecules were run for each model i.e., a total of 16 different combinations were simulated.

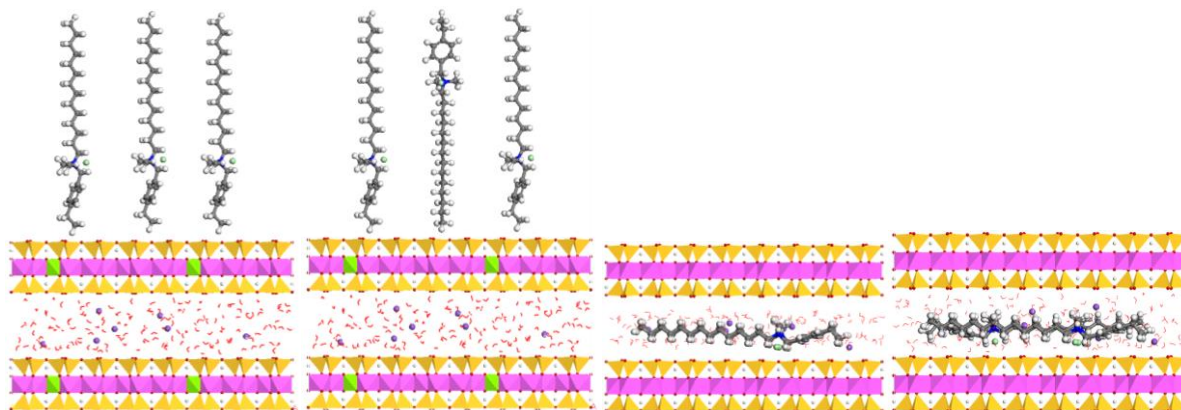


Fig. 2. Directions and positions (configurations) of TDEBAC molecules on Na-MMT within interlayer water and sodium ions. Colors representing red (oxygen); white (hydrogen); yellow (silicon); green (magnesium and chlorine); purple (sodium); and pink (aluminum; surface waters are deleted for clarity (only 4 configurations of 16 was randomly selected)

2.2. Forcefield assignment

In our models, TDEBAC exists as an organic compound and has covalent bonds which prevents the use of CLAYFF (Cygan et al., 2004) parameters. That is why all the entire 16 configurations were parameterized by Consistent Valence Forcefield (CVFF) (Dauber-Osguthorpe et al., 1988). Water molecules were assigned by SPC/E charges of Berendsen (Berendsen et al., 1987) to provide better flexibility of potential energy and full interaction between water-clay-surfactant phases (Zhao and Burns, 2012). Eventually, the water oxygen and hydrogen charges were set to -0.848 and 0.428, respectively. In addition, a unit cell charge for all models were calculated for different cases as; -0.600 (no substitution), -0.469 (85 CEC), -0.572 (118 CEC) and -0.563 (151 CEC), respectively. All these values are consistent with the study of Tambach (Tambach et al., 2006). If the substitution occurs in two sheets (tetrahedral/octahedral), a unit cell layer charge is -0.625. Sodium cation was added to make total charge zero (neutral) for all supercells.

2.3. Simulation

Sixteen models were dynamically simulated to understand the CEC capacity, basal spacing and interactions between three components, i.e. Na-MMT, TDEBAC, and water. For this purpose, after parameterization, energy minimization by Steepest Descent method was performed to get rid of all possible irregularities and reach a relaxed geometry without any overstretched bonds and very closely spaced atoms. Besides, Ewald (Ewald, 1921) summation was switched on to determine both electrostatic and van der Waals energies within 0.01 kcal/mol accuracy and 0.001 convergence criterion for all lattices. Molecular dynamic simulation steps were started upon energy minimization step. Berendsen thermostat (Berendsen et al., 1984) and Andersen barostat (Andersen, 1980) methods were then switched on to re-scale the velocities and coordinates of particles and control the temperature (298.0 K) and pressure. The position of all particles was integrated by Velocity Verlet algorithm (Swope et al., 1982). As it is well-known, volume is a dynamic phenomenon and changes during the experimental studies, but pressure is a constant variable in experiments. Thus isothermal-isobaric ensemble (constant

temperature, pressure, and number of molecules), shortly known as NPT ensemble was used to simulate models with 1 femtosecond (fs) time step. We used Discover module for all simulations. Simulations of 1 nanosecond (ns) were performed with periodic boundary conditions.

2.4. Analysis

Adsorption mechanism of TDEBAC on montmorillonite in aqueous media with different CEC was analyzed by means of characterization tests such as FT-IR, XRD, RDF and MSD. In addition to these analyses, H-bonds and chain-chain interactions were also explained by output snapshots during simulation. Moreover, we calculated the surfactant binding energies for all models using Eq. 2 as follows:

$$E_{BE} = (E_{ORGANO-MMT}) - [E_{MMT} + E_{SURFACTANT}] \quad (2)$$

where E_{BE} binding energy of each configuration and $E_{ORGANO-MMT}$ is the total potential energy of each organo-MMT configuration, E_{MMT} and $E_{SURFACTANT}$ are potential energies of individual montmorillonite and TDEBAC molecule in kcal/mol unit. All basal surface water molecules were deleted as binding energy calculations were performed. Finally, X-ray diffraction patterns within Bragg's Law (Eq. 3) were calculated for selected models by Reflex tools situated in Materials Studio to comprehend the importance of CEC in organo-MMT composites.

$$nx\lambda = 2dx(\sin \theta) \quad (3)$$

where n is an integer, λ is the wavelength of incident wave, d is the spacing between the planes in the atomic lattice, and θ is the angle between the incident and the scattered beams.

Diffusion coefficients of TDEBAC surfactant for each configuration at 298 K was calculated by Einstein relation (Peskir, 2003) using the mean square displacement (MSD). In this case, the Einstein relation can be described as:

$$Slope=2dDt \quad (4)$$

where d is the number of dimensions ($d=2$), for the diffusion in interlayer space (Zhao and Burns, 2012), t is the time for the slope interval ($t=1ns$) and D is diffusion coefficient in cm^2/s .

3. Results and discussion

Molecular dynamics simulations were carried out for Na-MMT at four different cation exchange capacities and four different configurations of quaternary ammonium surfactant within the explicit water molecules; this means that three TDEBAC surfactants were located on basal and interlayer spaces with two of their polar heads facing in the same direction and the middle one facing in the opposite direction. Therefore, we basically have two models for review: i) surfactant adsorption on basal surface, and ii) surfactant interaction and its effect on intercalation. For this purpose, we simulated the effect of TDEBAC on basal spacing and analyzed its different impacts on basal and interlayer surfaces. Chain-chain interactions were also studied with the final simulated geometries. The importance of sodium and chlorine ions for adsorption behavior of surfactants was examined as well. For all these investigations, FT-IR, XRD, RDF and MSD analyses were conducted. In the subsequent section, only the surfactant within the opposite direction placed in the interlayer was selected to be compatible with each other. The results for other configurations are discussed in each respective section.

3.1. FT-IR analysis

First, surfactant adsorption densities onto Na-MMT at all CEC ratios were calculated. As mentioned in our previous study (Karataş et al., 2013), the infrared (IR) spectrophotometer is a commonly used tool to study gas and liquid adsorption on solid surfaces. In this study, FT-IR spectra were computed by Discover module. All configurations of four models including surfactants were rebuilt without any water molecules placed on basal surfaces followed by computing the spectra. The purpose of FT-IR process was to understand surfactant penetration and adsorption on Na-MMT surfaces. Spectrum analyses were conducted for all the models against CEC values. All calculated wavenumbers and experimental values are presented in Table 1.

As mentioned in Table 1, five different structures were analyzed and compared with the experimental results cited elsewhere (Erkan et al., 2010; Navratilova et al., 2007). All experimental wavenumbers are characteristic for Na-MMT. 'DRY untreated' structure means no surfactant and water molecules present in each model. For other four models, interlayer water and surfactants exist in Na-MMT. As shown in Table 1, the computed spectra are generally consistent with the experimental wavenumbers. For example, Al-O-Si deformation at 524 cm⁻¹ was observed approximately at 514 cm⁻¹ for all structures except 151 CEC model. One characteristic peak for Na-MMT is Si-O-Si peak at 992 cm⁻¹ which was seen to shift 5 cm⁻¹ to the right for all calculated organo-MMT structures. However, for this particular peak, "no substitution" and "DRY untreated" models respectively shifted to the left at 6 and 8 cm⁻¹. Another significant vibration is water hydroxyl deformation at 1634 cm⁻¹ which induced a shift of nearly 13 cm⁻¹ for all models. Other prominent peak for Na-MMT is -OH stretching of structural hydroxyl group, observed at two points: one is at the same peak for all models, but the other is at 10 cm⁻¹ left shifting point except DRY untreated model (insufficient information related to FT-IR to compare it with XRD peaks). All these deflections and shifts are indicative of surfactant adsorption on Na-MMT. Besides, two marked and evident peaks point out well-known organo-MMT wavenumbers at 2854 and 2928 cm⁻¹. At these points, no pronounced shift or change is recorded for any kind of clay minerals. That's why for all organo-MMT models, asymmetric C-H stretching is characteristic of these spectra for surfactants and observed at 2914 and 2978 cm⁻¹ wavenumbers, respectively.

Table 1. FT-IR wavenumbers for all models and experiments

DRY untreated	Calculated peaks (cm ⁻¹) vs. CEC				Exp.* (cm ⁻¹)	Assignment
	No subs.*	85	118	151		
514	514	511	513	519	524	Al-O-Si deformation
627	628	626	621	618	621-626	Al-O and Si-O stretching
684-699	686-699	687-697	688-694	684-697	695-707	Si-O stretching
713-727	721	721	727	727	726	OH deformation
790	791	790	789	783	790	Si-O stretching
900-916	900-917	902-915	903-915	907-910	911	Al-Al-OH deformation
984	986	987-992	998	997	992	Si-O-Si stretching
1125	1101	1119	1121	1119-1122	1115	Si-O-Si stretching
1198	1209	1201-1208	1198-1207	1203-1210	1200-1206	OH stretching of structural hydroxyl groups
1637-1656	1638-1659	1641-1654	1643-1656	1640-1647	1634	OH deformation of water
No TDEBAC peak	2914	2914	2914	2915	2854**	Alkyl asymmetric C-H stretching
No TDEBAC peak	2978	2978	2978	2979	2928**	Alkyl asymmetric C-H stretching
3624	3613-3624	3617-3624	3613-3624	3817-3628	3625	OH stretching of structural hydroxyl groups

* Characteristic peaks for pure and organo-montmorillonite as modified by any kind of quaternary ammonium surfactants.

** Experimental peaks were taken from Erkan et al. (Erkan et al., 2010) previous study

Interestingly, Table 1 illustrates that DRY untreated MMT model shows approximately the same wavenumbers with those experimental data on Na-MMT (Erkan et al., 2010). In addition, the other models are obviously consistent with the experimental results. 118 CEC model appears to present the best match with the experimental wavenumbers.

3.2. XRD and basal spacing analysis

X-ray diffraction patterns were calculated during the simulation to clarify the basal spacing and importance of CEC ratios on intercalation. All results are given in Fig. 3. The peaks are for those surfactants placed between layer models as mentioned above.

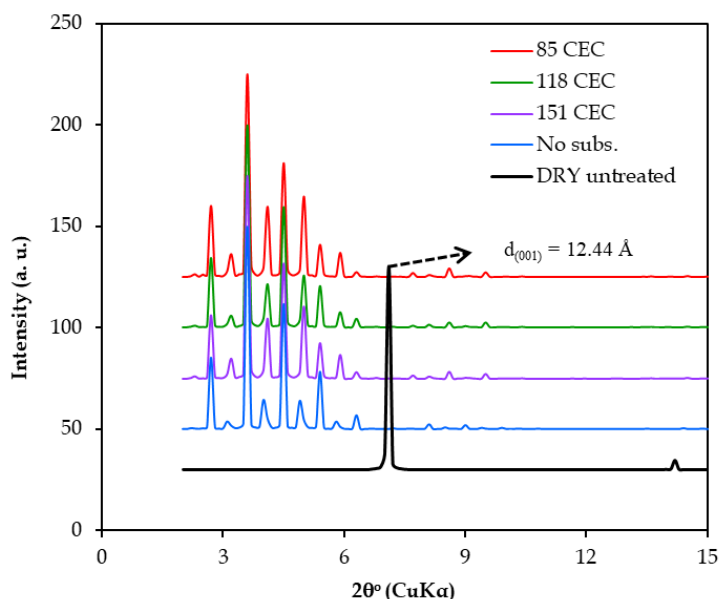


Fig. 3. XRD patterns of the surfactant located between layers for all models and dry untreated MMT

As shown in Fig. 3, all XRD peaks shifted to the left compared to the dry untreated MMT. Interestingly, the shift was more pronounced with increasing the CEC ratio. These observations were verified by the previous experimental studies (He et al., 2006a; Yoshimoto et al., 2005; Zhu et al., 2011). For example, Xi et al. studied organically modified and intercalated SWy-MMT with a quaternary ammonium surfactant “octadecyltrimethyl ammonium bromide” to explain changes in surface properties (Xi et al., 2007). In their study increasing the CEC ratios the XRD peaks shifted to the left and basal spacing increased from 12 to 20.30 Å. Likewise, He et al. reported basal spacing values of 12.8 for pure MMT and 14.8, 19.8 and 22.60 Å for three different HTAB concentrations, respectively (He et al., 2006a). In addition to these experimental studies, two theoretical investigations (Cygan et al., 2009; Heinz et al., 2006) were conducted to explain surfactant incorporation into basal spacing of layered materials and MMT. Cygan et al. found in their MD studies the basal spacing of modified MMT (CEC=91 meq/100g) by octadecylammonium to rise to 30 Å (Cygan et al., 2009). The other MD study performed by Heinz et al. studied effect of chain length, head group structure, and cation exchange capacity (91 meq/100g and 145 meq/100g) onto modified alkylammonium MMT (Heinz et al., 2006). They found the basal spacing for the low and high CEC ratios to increase to 18.5 Å and 24 Å for the quaternary head groups of 14 CH₂ chain which is like the surfactant used in this study. Then again, the basal spacing shown in Fig. 3 for the ‘DRY untreated’ MMT, (001) plane is 12.44 Å. Surfactant positioned into the interlayer of the three models CEC’s, basal spacing in all the six configurations, changed in the range of 21.60 and 24.47 Å due to the directions of surfactant and CEC values. However, this value is around 19.77 Å for the “no subs.” configurations where 2θ° angle is 4.47°, as shown in blue line in Fig. 3. However, when the three surfactant molecules are placed within clay layers either in the same direction or in the middle one in the opposite direction, clay exhibits swelling. As seen in Fig. 3, the basal spacing has expanded by shifting to the left. Also, as the CEC has increased, the peaks have become more pronounced but with little differences among them because the maximum basal spacing value at the most intensified point of 2θ° = 3.6 for the four models has been calculated as 24.52 Å. Despite increase in CEC, the lack of proportional increase in basal spacing is ascribed to the insufficient number of surfactant molecules.

On the other hand, as indicated in Fig. 3, for the surfactant located on to the basal surface model the trend is the same but the basal spacing is 16.30 Å for all six configurations including CEC of 85, 118 and

151. Interestingly, this value does not change for “no subs.” configurations as compared with the previous model. Eventually, as surfactant penetrated the interlayer space, the basal spacing increased by 3.4 Å as mentioned in the experimental studies. In summary, surfactants located in the interlayer space cause more intercalation than those surfactants positioned on the basal space due to the swelling of Na-MMT.

The XRD peaks obtained upon placing the surfactant configurations into the basal space of clay as before and simulated after 1 ns are presented in Fig. 4. As evident from Fig. 4, when the surfactants are accommodated on the basal surface, the shifts of peaks to the left have become more pronounced; this is attributed to the increase in the basal spacing of clay. However, due to the surfactant configurations at the basal space, the intensity of peaks have changed and yielded a calculated maximum peak value of $2\theta = 2.3$ as 38.38 Å. Interestingly, more layering tendency was noted when more surfactant was placed on the basal plane. One reason for this is that during simulations, despite the presence of water molecules, the double layer of clay inclined towards the polar head of the surfactant. The other reason is because the surfactant molecules positioned themselves within the layers. As shown in Table 2, surfactant has strongly bound to the clay surfaces leading to more stable layers. Since under experimental conditions, adsorption at basal space and inter layers simultaneously occurs, completion of monolayer coverage through penetration of each surfactant into basal space improves both swelling and intercalation. In addition, as seen in Fig. 4, there appears to be an increase in shifting of the peaks to the left with increasing the CEC but due to the absence of sufficient number of surfactants, no definitive conclusion was arrived.

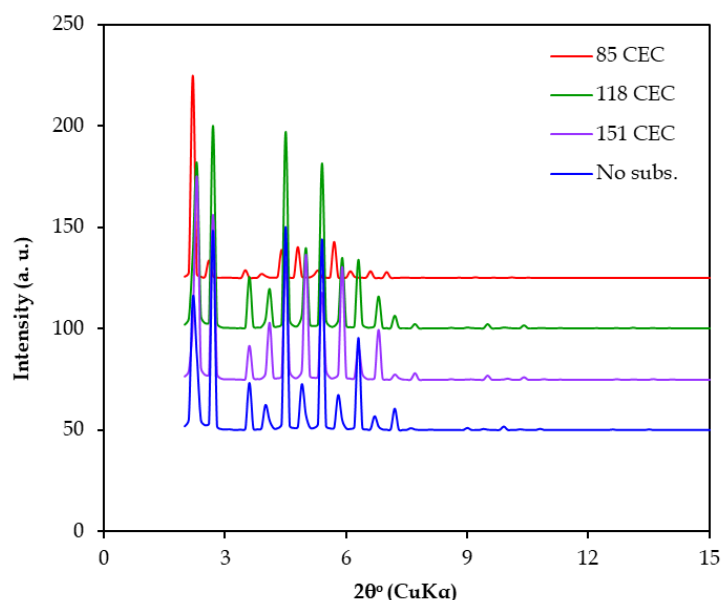


Fig. 4. XRD patterns for surfactants placed on to basal surfaces for all models

3.3. RDF Analysis

Radial distribution functions (RDF) were analyzed by Forcite module after simulations to explain the probability of finding any kind of atoms at any reference atom distances. Interactions between species in the selected distances due to the RDF analysis were explained and sorptive characteristic of surfactants were revealed. Towards this aim, interactions between water hydrogen and tetrahedron silica oxygen, and sorption properties of surfactant chain carbon and water hydrogen radial distribution functions of surfactant within the opposite direction configurations between interlayer were respectively calculated and presented in Figs. 5 and 6. In Fig. 5, at short distances around 2-4 Å, water hydrogen showed a high interaction with surface oxygen for all models due to the hydrophilic nature of clay surface. Therefore, there is an intense H-bond between water and tetrahedron oxygen. As the distance is increased, RDF oscillation reaches a constant value around 13 Å, and no significant interaction between water and clay surfaces at long distances is expected.

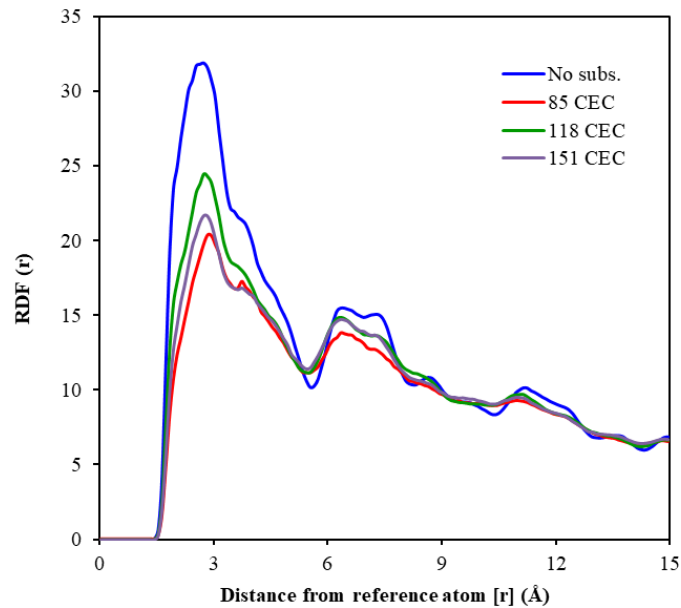


Fig. 5. Average Radial distribution functions of surface water hydrogen and surface silica tetrahedron oxygen after 1 ns NPT simulation

Another observation is about the CEC ratios. As seen in Fig. 5, RDF presents the highest value at 3 Å for no substitution structure. On the other hand, increasing the CEC ratio from 85 to 151 increased RDF at short distances yielding smallest and highest basal spacing and intercalation, respectively. Therefore, because the basal spacing for 85 CEC structure gives the lowest peak, it indicates that water molecules adsorb on clay surfaces less than the other models. The RDF values for water of surfactant configurations in the same direction in the interlayer are 24, 19, 25 and 23 at 2-3 Å distances. On the other hand, the probabilities of the water molecules at short distances for all the CEC structures are less for oppositely directed surfactant configurations. The average RDF for carbon in surfactant chain and water hydrogen was calculated to explain the probability of each surfactant penetrated the interlayer (Fig. 6). At short distances of around 3-5 Å, for all structures, surfactant aliphatic carbon produced an interaction with water molecules but not as much as those between water and clay surfaces due to the hydrophobic interactions of chains. As seen in Fig. 6, the highest interaction occurs around 7-8 Å for 85 CEC structure. This means that at short distances and at the lowest CEC ratio, RDF presents the highest

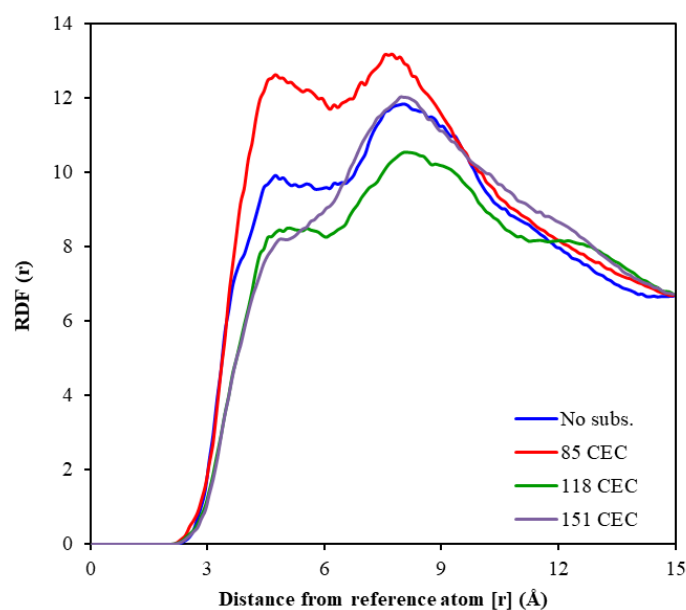


Fig. 6. Average RDF of basal space models for surfactant chain aliphatic carbon and water hydrogen

value due to the more interaction between carbon and water hydrogen closest to the surface. Similarly, 118 CEC structure provides the highest interaction due to the lesser water molecules found at these distances.

On the other hand, surfactant within the same direction in interlayer configurations has the same trend for each structure. However, RDF values at 3-5 Å distances were calculated as 12, 11, 13 and 9 for 'no subs', 85, 118 and 151 CEC configurations, respectively. These results indicate that no substitute, 85 and 151 CEC structure surfactant chain has nearly the same interaction except 118 CEC structure. The probability of finding surfactant in the same direction carbon chain exhibits higher interactions than the oppositely directed configurations. Among 7-8 Å distances, RDF values changed to 13, 12, 10 and 12 for the same configurations (The highest RDF values among 7-8 Å distances are 13 (85 CEC), 12 (No subs., 151 CEC), and 10 (118 CEC)).

The probability of TDEBAC located in the interlayer configurations and surfactant positioned in basal surfaces are examined and discussed below. First, probabilities of the water hydrogen and basal surface oxygen were calculated. RDF values for the surfactant in the opposite direction on basal surfaces is around 14, 24, 16 and 13, respectively, for 'no subs', 85, 118 and 151 CEC configurations at 4-5 Å distance. Likewise, RDF data for the surfactant in the same direction is 14, 12, 17 and 15, respectively. These RDF data show that interactions between water and Na-MMT surface increase for 118 and 151 CEC structures but decrease dramatically for 85 CEC configurations (The values mentioned above are not plotted for the sake of brevity).

The second RDF calculation was performed between aliphatic chain carbon and water hydrogen. RDF for surfactant in the opposite direction is 2, 5, 2 and 1.5 Å and that for the surfactant in the same direction configurations for 'no subs', 85, 118 and 151 CEC is 9, 3, 8 and 2 Å, respectively. Interactions for all structures except 85 CEC are higher than surfactant in the opposite direction. It means that the probability of finding a surfactant in the same direction configurations is more favorable than the reversed position configurations due to both H-bonding of polar groups and hydrophobic chain interactions. All these RDF values show that probability of finding surfactant at short distances located onto basal surfaces present a less energetic interaction due to the nature of adsorption being spontaneous and physical.

It is known in the literature that adsorbing due to increasing CEC also increases (He et al., 2006b; Liu and Xiao, 2012; Pan and Shen, 2007; Vazquez, 2008). The reason why the motif with 85 CEC has the least interaction compared to 118 and 151 CEC in Fig.5 suggests that the polarity of water molecules with each other may increase due to the interaction of surfactants with different morphologies on the surface for this motif. To confirm this, Fig.6 considering the hydrophobicity in Figure 6, attention was paid to the interaction of the hydrophobic tails of the surfactant with the water molecules, and here, contrary to Fig.5, higher interaction was observed in the model with 85 CEC. From here, it shows that the interactions of the hydrophilic heads with the basal surfaces of the clay increase. As a matter of fact, these findings were observed in animations throughout the simulation and parallel results were obtained in the binding energy results.

3.4. MSD analysis

In the present study, we calculated the diffusion coefficient for each surfactant by Forcite module for last 1 ns simulation, equivalent to 20000 frames. Using the Einstein equation, the diffusion coefficients of TDEBAC for each structure were calculated as 1.98×10^{-6} , 2.86×10^{-6} , 3.46×10^{-6} and 2.88×10^{-6} cm²/s for No subs., 85, 118 and 151 CEC, respectively. All the coefficients imply that the diffusivity of surfactant increases with increasing the CEC ratio. Moreover, the results explain the mobility of head and chain groups of the surfactant. Namely, in the early stages of the simulation, surfactant polar head group including nitrogen plays a major role on the diffusion through H bonding via clay surface and water molecules. During the monitoring MD frames, in the early stages such as first 200 ps, the interactions between each chain group of surfactants composed of 14 ethyl (CH₂) increases because their hydrophobic groups cause surfactant diffusion. Likewise, diffusion coefficients of TDEBAC for the other interlayer configurations (all head groups in the same direction) were computed as 2.50×10^{-6} , 2.94×10^{-6} , 2.62×10^{-6} and 1.65×10^{-6} cm²/s, respectively.

On the other hand, diffusivities of surfactant in the same direction but on the basal surfaces were found as 7.44×10^{-6} , 5.77×10^{-6} , and 4.02×10^{-6} and 6.91×10^{-6} cm^2/s . For the remaining last four configurations, surfactant positioned in opposite direction, MSD's were calculated as 5.28×10^{-6} , 5.16×10^{-6} , and 6.02×10^{-6} and 8.57×10^{-6} cm^2/s . All the results for the surfactant on basal model show that surfactant in the opposite direction creates a more mobile medium than the others. In addition to this observation, comparison of the models indicates that diffusivity of surfactant on basal surface is faster than the other models.

3.5. Binding energy results

As illustrated in Table 2, the binding (adsorption) energy for each configuration without any water molecules was calculated to better explain the surfactant adsorption onto Na-MMT surfaces.

Table 2. Binding energy results for each structure in kcal/mol

Structures	basal surface		interlayer surface	
	same direction	middle reversed	same direction	middle reversed
No subs.	-248.88	-194.98	-621.98	-639.80
85 CEC	-24.82	-230.68	-273.15	-458.13
118 CEC	-678.18	-34.86	-688.90	-525.63
151 CEC	-105.12	+86.46	-503.94	-519.41

As demonstrated in Table 2, considering surfactant on basal surface model, binding energies were found to decrease substantially for all structures except 85 CEC. For the interlayer surface model, however, TDEBAC binding on 85 CEC continued to rise though the trend of binding for other structures did not change except 151 CEC. Another important finding shown in Table 2 is that the interlayer surface model exhibited a huge difference compared to the other model. For example, for no subs. structure, while binding energy was -248.88 kcal/mol for TDEBAC on basal surface within the same direction, it became -621.98 kcal/mol for the interlayer surface configuration. Other significant inference, as shown in Table 2, is about surfactant directions, which adversely affect the binding. For example, as reported in Table 2 and illustrated in Fig. 7, while binding energies for 118 CEC are -678.18 and -688.90 kcal/mol for surfactant in the same directions, these values were reduced to -34.86 and -524.50 kcal/mol for surfactant configuration in opposite direction, respectively.

As indicated on the left side caption of Fig. 7, since TDEBAC was initially positioned within the same direction on the basal surface of Na-MMT, all three of the surfactants tended to remain on the surface due to the H-bonds. On the other hand, as the surfactant direction in the middle was reversed, TDEBACs moved away from the surface due to the chain-chain interaction; that is the reason for the dramatic decrease observed in binding energy. Otherwise, binding energies generally increased as the CEC ratios increased until 118 meq/100g but decreased until 151 CEC. Two important scenarios can be speculated: one is the lack of number of surfactants and the other one is that of hydrophobic interactions of surfactant chains. Fig. 8 provides a better understanding of the final configuration of surfactant in the opposite direction on basal surface.

As shown in Fig. 8, two of TDEBAC surfactant molecules bind each other due to the hydrophobic interaction and thus are desorbed from the surfaces. Therefore, the free energy of binding for the given configuration is +86.46 kcal/mol, as given in Table 2. Interestingly, all interlayer water molecules due to the hydrogen bond between silica surfaces exhibited two layers, as indicated in Fig. 7 and 8.

In two of the important experimental studies supporting the modeling analyses, in the light of thermal and chemical analyses, it was revealed that as the CEC capacity increases, the amount of adsorption increases as well as basal spacing and peak shifts (He et al., 2005; Vazquez, 2008). In another experimental study, authors stated that the distribution and arrangement of surfactant in the

organoclays control sorption efficiency and mechanism rather than BET-N₂ surface area, pore volume, or pore diameter (He et al., 2006b).

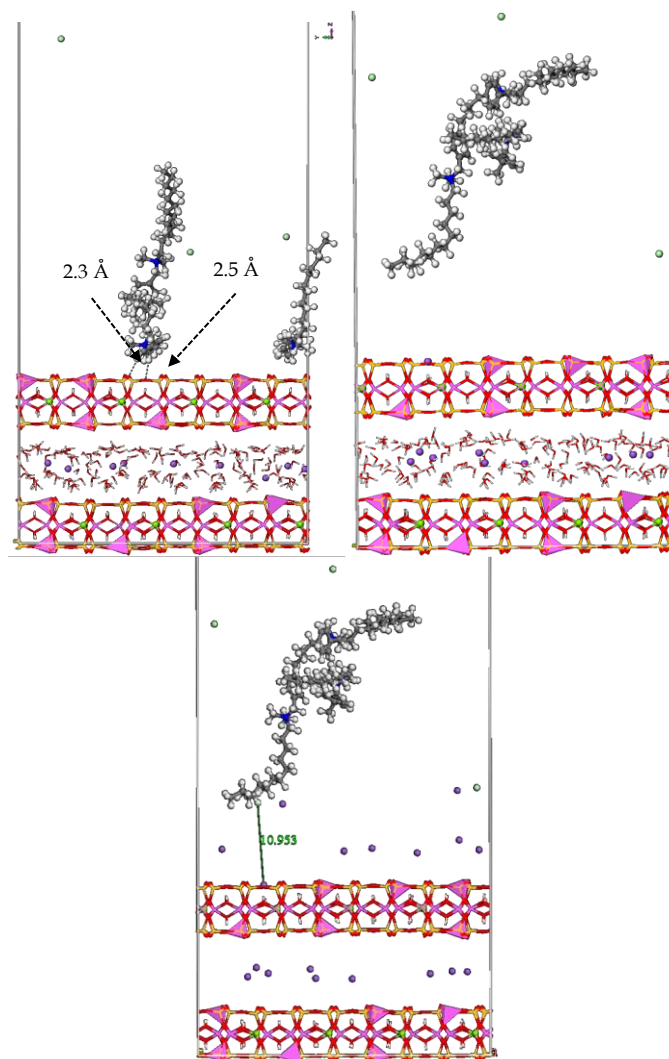


Fig. 7. Final position of surfactant within the same (left side) and opposite direction (right side) on basal surface of 118 CEC Na-MMT within the interlayer water (surface waters are deleted for clarity)

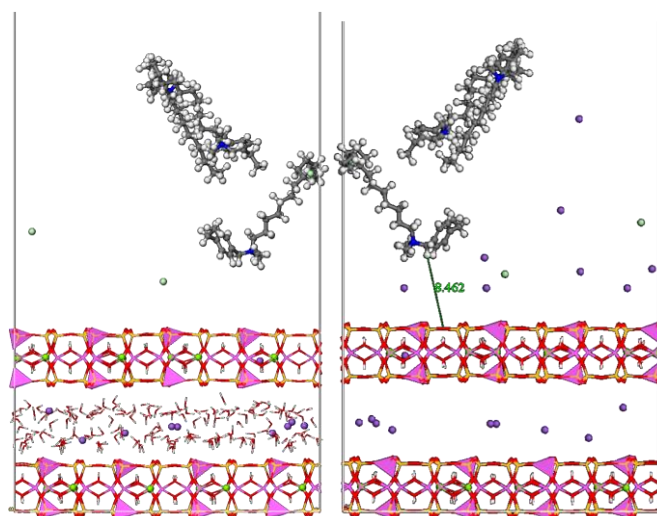


Fig. 8. Final configuration of surfactant within the opposite direction on basal surface of 151 CEC Na-MMT within the interlayer water (surface waters are deleted for clarity)

4. Conclusions

MD simulation was investigated to identify the mechanism of quaternary ammonium surfactant coded as TDEBAC uptake on basal and interlayer spaces for different CEC ratios of Na-MMT. The main parameters were location and direction of surfactant and water molecules on both basal and interlayer. In addition, MD results illustrated that morphology of Na-MMT was another important parameter. Simulation results confirmed that the arrangement (direction and location) of the surfactants controlled the adsorption mechanism of organoclays. Surfactant adsorption on clay surface was mainly due to H-bonding between hydrogen of the surfactant and oxygen of the clay surface and hydrophobic interactions of chain groups. Electrostatic interaction between chlorine (Cl^{-1}) and sodium ions (Na^{+1}) was another observation made during simulations especially for the basal surface model. All results showed that two possible models can occur for the position of the surfactant during the actual experiments. One was surfactant on basal and the other one was in interlayer surface of Na-MMT clay. In summary, simulations based on structural properties as XRD, RDF and FT-IR and dynamic properties as MSD reveal that adsorption of TDEBAC molecule increases until CEC of 118 but above this CEC value desorption is apparent. The surface properties of Na-MMT such as swelling, intercalation and surface activity are generally improved leading to an organophilic state (Hua-Bin and Han-Ning, 2012) whereas increasing CEC to 151 deteriorated the structural and dynamic properties of Na-MMT; these MD results are in accord with the experimental and theoretical results.

Acknowledgements

The financial support for this work from TUBITAK-BIDEB 2214/A scholarship program (The Scientific and Technological Research Council of Turkey- Science Fellowships and Grant Programs Department) is gratefully acknowledged. Computing resources used in this work were provided by Department of Chemical and Materials Engineering (CME) at University of Alberta.

References

- ANDERSEN, H. C., 1980. *Molecular dynamics simulations at constant pressure and/or temperature*. J Chem Phys, 72.
- BERENDSEN, H. J. C., GRIGERA, J. R. & STRAATSMA, T. P., 1987. *The Missing Term in Effective Pair Potentials*. J Phys Chem-U.S., 91, 6269-6271.
- BERENDSEN, H. J. C., POSTMA, J. P. M., VANGUNSTEREN, W. F., DINOLA, A. & HAAK, J. R., 1984. *Molecular-Dynamics with Coupling to an External Bath*. J Chem Phys, 81, 3684-3690.
- BREEN, C., WATSON, R., MADEJOVÁ, J., KOMADEL, P. & KLAPYTA, Z., 1997. *Acid-Activated Organoclays: Preparation, Characterization and Catalytic Activity of Acid-Treated Tetraalkylammonium-Exchanged Smectites*. Langmuir, 13, 6473-6479.
- CYGAN, R. T., GREATHOUSE, J. A., HEINZ, H. & KALINICHEV, A. G., 2009. *Molecular models and simulations of layered materials*. Journal of Materials Chemistry, 19, 2470.
- CYGAN, R. T., LIANG, J.-J. & KALINICHEV, A. G., 2004. *Molecular Models of Hydroxide, Oxyhydroxide, and Clay Phases and the Development of a General Force Field*. The Journal of Physical Chemistry B, 108, 1255-1266.
- DAUBER-OSGUTHORPE, P., ROBERTS, V. A., OSGUTHORPE, D. J., WOLFF, J., GENEST, M. & HAGLER, A. T., 1988. *Structure and energetics of ligand binding to proteins: Escherichia coli dihydrofolate reductase-trimethoprim, a drug-receptor system*. Proteins, 4, 31-47.
- DE PAIVA, L. B., MORALES, A. R. & VALENZUELA DÍAZ, F. R., 2008. *Organoclays: Properties, preparation and applications*. Applied Clay Science, 42, 8-24.
- ERKAN, İ., ALP, İ. & ÇELİK, M. S., 2010. *Characterization of Organo-Bentonites Obtained from Different Linear-Chain Quaternary Alkylammonium Salts*. Clays and Clay Minerals, 58, 792-802.
- ERSOY, B. & ÇELİK, M. S., 2003. *Effect of hydrocarbon chain length on adsorption of cationic surfactants onto clinoptilolite*. Clays and Clay Minerals, 51, 172-180.
- EWALD, P. P., 1921. *Die Berechnung optischer und elektrostatischer Gitterpotentiale*. Annalen der Physik, 369, 253-287.
- FERMEGLIA, M., FERRONE, M. & PRICL, S., 2003. *Computer simulation of nylon-6/organoclay nanocomposites: prediction of the binding energy*. Fluid Phase Equilib, 212, 315-329.
- HANG, P. T. & BRINDLEY, G. W., 1970. *Methylene blue adsorption by clay minerals. Determination of surface areas and cation exchange capacities*. Clays and Clay Minerals, 18, 203-212.

- HE, H., DING, Z., ZHU, J., YUAN, P., XI, Y., YANG, D. & FROST, R. L., 2005. *Thermal characterization of surfactant-modified montmorillonites*. *clays and clay minerals*, 53, 287-293.
- HE, H., FROST, R. L., BOSTROM, T., YUAN, P., DUONG, L., YANG, D., XI, Y. & KLOPROGGE, J. T., 2006a. *Changes in the morphology of organoclays with HDTMA⁺ surfactant loading*. *Applied Clay Science*, 31, 262-271.
- HE, H., MA, Y., ZHU, J., YUAN, P. & QING, Y., 2010. *Organoclays prepared from montmorillonites with different cation exchange capacity and surfactant configuration*. *Applied Clay Science*, 48, 67-72.
- HE, H., ZHOU, Q., MARTENS, W. N., KLOPROGGE, T. J., YUAN, P., XI, Y., ZHU, J. & FROST, R. L., 2006b. *Microstructure of HDTMA⁺-modified montmorillonite and its influence on sorption characteristics*. *Clays and Clay Minerals*, 54, 689-696.
- HEINZ, H. & SUTER, U. W., 2004. *Atomic Charges for Classical Simulations of Polar Systems*. *The Journal of Physical Chemistry B*, 108, 18341-18352.
- HEINZ, H., VAIA, R. A., KRISHNAMOORTI, R. & FARMER, B. L., 2006. *Self-Assembly of Alkylammonium Chains on Montmorillonite: Effect of Chain Length, Head Group Structure, and Cation Exchange Capacity*. *Chemistry of Materials*, 19, 59-68.
- HUA-BIN, L. & HAN-NING, X., 2012. *Investigation on Intercalation Modification of Sodium-montmorillonite by Cationic Surfactant*. *Journal of Inorganic Materials*, 27, 780-784.
- KARATAŞ, D., TEKIN, A. & ÇELİK, M. S., 2013. *Adsorption of quaternary amine surfactants and their penetration into the intracrystalline cavities of sepiolite*. *New Journal of Chemistry*, 37, 3936.
- LIU, H.-B. & XIAO, H.-N., 2012. *Investigation on Intercalation Modification of Sodium-montmorillonite by Cationic Surfactant*. *Journal of Inorganic Materials*, 27, 780-784.
- LIU, X., LU, X. C., WANG, R. C., ZHOU, H. Q. & XU, S. J., 2009. *Molecular dynamics insight into the cointercalation of hexadecyltrimethyl-ammonium and acetate ions into smectites*. *American Mineralogist*, 94, 143-150.
- MAES, A., STUL, M. S. & CREMERS, A., 1979. *Layer Charge-Cation-Exchange Capacity Relationships in Montmorillonite*. *Clays and Clay Minerals*, 27, 387-392.
- MARKARIAN, J., 2005. *Automotive and packaging offer growth opportunities for nanocomposites*. *Plastics, Additives and Compounding*, 7, 18-21.
- MERINSKA, D., MALAC, Z., POSPISIL, M., WEISS, Z., CHMIELOVA, M., CAPKOVA, P. & SIMONIK, J., 2002. *Polymer/clay nanocomposites based on MMT/ODA intercalates*. *Composite Interfaces*, 9, 529-540.
- NAVRATILOVA, Z., WOJTOWICZ, P. E., VACULIKOVA, L. & SUGARKOVA, V., 2007. *Sorption of alkylammonium cations on montmorillonite*. *Acta Geodynamica et Geomaterialia*, 4, 59-65.
- PAN, C. & SHEN, Y.-H., 2007. *Estimation of Cation Exchange Capacity of Montmorillonite by Cationic Surfactant Adsorption*. *Communications in Soil Science and Plant Analysis*, 34, 497-504.
- PESKIR, G., 2003. *On the diffusion coefficient: The Einstein relation and beyond*. *Stoch Models*, 19, 383-405.
- SWOPE, W. C., ANDERSEN, H. C., BERENS, P. H. & WILSON, K. R., 1982. *A Computer-Simulation Method for the Calculation of Equilibrium-Constants for the Formation of Physical Clusters of Molecules - Application to Small Water Clusters*. *J Chem Phys*, 76, 637-649.
- TAMBACH, T. J., BOEK, E. S. & SMIT, B., 2006. *Molecular order and disorder of surfactants in clay nanocomposites*. *Phys Chem Chem Phys*, 8, 2700-2.
- TANAKA, G. & GOETTLER, L. A., 2002. *Predicting the binding energy for nylon 6,6/clay nanocomposites by molecular modeling*. *Polymer*, 43, 541-553.
- THENG, B. K. G., CHURCHMAN, G. J., GATES, W. P. & YUAN, G. 2008. *Organically Modified Clays for Pollutant Uptake and Environmental Protection*. In: HUANG, Q., HUANG, P. M. & VIOLANTE, A. (eds.) *Soil Mineral Microbe-Organic Interactions*. Berlin, Heidelberg: Springer, .
- VAZQUEZ, A., 2008. *Modification of montmorillonite with cationic surfactants. Thermal and chemical analysis including CEC determination*. *Applied Clay Science*, 41, 24-36.
- VIANI, A., GUALTIERI, A. F. & ARTIOLI, G., 2002. *The nature of disorder in montmorillonite by simulation of X-ray powder patterns*. *American Mineralogist*, 87, 966-975.
- XI, Y., ZHOU, Q., FROST, R. L. & HE, H., 2007. *Thermal stability of octadecyltrimethylammonium bromide modified montmorillonite organoclay*. *Journal of colloid and interface science*, 311, 347-53.
- YOSHIMOTO, S., OHASHI, F. & KAMEYAMA, T., 2005. *X-ray diffraction studies of intercalation compounds prepared from aniline salts and montmorillonite by a mechanochemical processing*. *Solid State Commun*, 136, 251-256.
- ZENG, Q. H., YU, A. B., LU, G. Q. & STANDISH, R. K., 2003. *Molecular Dynamics Simulation of Organic-Inorganic Nanocomposites: Layering Behavior and Interlayer Structure of Organoclays*. *Chemistry of Materials*, 15, 4732-4738.

- ZHAO, Q. & BURNS, S. E., 2012. *Molecular dynamics simulation of secondary sorption behavior of montmorillonite modified by single chain quaternary ammonium cations*. *Environ Sci Technol*, 46, 3999-4007.
- ZHU, J., WANG, T., ZHU, R., GE, F., YUAN, P. & HE, H., 2011. *Expansion characteristics of organo montmorillonites during the intercalation, aging, drying and rehydration processes: Effect of surfactant/CEC ratio*. *Colloids and Surfaces A: Physicochemical and Engineering Aspects*, 384, 401-407.